Supporting Information

Muntyan et al. 10.1073/pnas.1417071112

SI Materials and Methods

Bacterial Strains and Growth Conditions. For the basic study the bacterial strains were cultivated under aerobic conditions in a circulatory shaker (300 rpm) in mineral liquid nutritional media (150 mL per 2-L flask). *Thioalkalivibrio versutus* AL2 was cultured at pH 10.0 and 30 °C in "soda" medium (1) using thiosulfate as a substrate, and *Paracoccus denitrificans*, strain AO1, and the WT strain (PD ID code 1222) were cultured at pH 7.0 and 32 °C in "phosphate" medium using 85 mM succinate as a source of carbon (2) up to the late exponential phase of growth at A_{660} = 3.4–3.9 (usually 16–18 h).

For the subsidiary comparative study of the expression level of the self-Coxs, cbb_3- and aa_3-type oxidases, the WT strain of *P. denitrificans* was grown under three diverse conditions specified earlier (3) and modified by us as described below: (*i*) aerobic conditions, in a rotary shaker at 400 rpm in round-shaped 1-L flasks filled with 10 mL of the growth medium containing 10 mM succinate; (*ii*) semiaerobic conditions, in a rotary shaker at 50 rpm in conical 50-mL glass flasks filled with 25 mL of the growth medium containing 25 mM succinate; and (*iii*) anaerobic conditions at static regime in 17-mL glass tubes closed with screw caps filled with 17 mL of the growth medium containing 25 mM succinate and 0.1 M $NaNO_3$. The bacterial cells used in the comparative study were harvested in the two phases of growth: the exponential phase at optical density of culture A_{660} = 0.5–0.6 in all growth conditions and the late exponential phase at optical density of culture A_{660} = 1.7–1.8 in aerobic conditions, A_{660} = 1.3–1.4 in semiaerobic conditions, and A_{660} = 1.4–1.6 in anaerobic conditions. An optical density (at 660 nm) was measured using spectrophotometer Specol-20 (Carl Zeiss).

Membrane Vesicle Isolation. For all experiments right-side-out membrane vesicles were isolated from freshly grown cells in isolation medium containing 50 mM CAPSO-KOH (pH 9.9), 50 mM K_2SO_4, 0.1 M sucrose, 0.1 mM EGTA, and 0.35 M Na_2SO_4 by disruption in a French press cell, according to standard procedures. Membranes were stored at −20 °C for up to a month without loss of enzymatic activity.

Na^+ Transport Measurements. For sodium (Na^+) transport experiments, starved bacterial cells exhausted of endogenous substrates were loaded with ^{22}Na (PerkinElmer Life Sciences) by incubating cells in the corresponding reaction medium containing 50 mM diethylamine (DEA) during 30 min on ice according to a previously reported protocol (4). Such incubation was repeated twice and then cells were washed two times with the cell reaction medium free from DEA. Membrane vesicles were loaded with ^{22}Na by mixing the stock samples containing protein at a concentration of 100 mg/mL with ^{22}Na, yielding counts of ∼1,440 cpm/μg of protein in the final mixture. Thereafter, vesicles in the mixture were allowed to load ^{22}Na by passive diffusion at 6 °C overnight in vesicle incubation medium B containing the appropriate buffer composition (50 mM CAPSO/Tricine/Mops-KOH, 50 mM K_2SO_4, 0.1 M sucrose, 0.1 mM EGTA, and 0.6 M Na_2SO_4). Na^+ transport was studied by incubating ^{22}Na-loaded bacterial cells or membrane vesicles in a 200-μL final volume of reaction mixture containing cell incubation medium A (50 mM CAPSO/Tricine/Mops-KOH and 0.62 M NaCl) or vesicle incubation medium B, respectively, at 22 °C. In both cases incubation medium contained only "cold" Na^+ before the experiments with Na^+-loaded cells or vesicles. Active Na^+ transport was started by addition of substrate to the reaction mixture. Thereafter, 25-μL samples were withdrawn from the incubation mixture at the desired time points and separated from the incubation medium by rapid (1–3 s) vacuum filtration through nitrocellulose filters (0.45 μm for cells or 0.22 μm for vesicles) (Millipore), followed immediately by washing with 1 mL of washing buffer. After washing, the filters containing samples were transferred to the inner wall of 1.5-mL Eppendorf tubes, then covered with 1 mL scintillation fluid (Ultima Gold mixture; PerkinElmer Life Sciences), mixed, and allowed to stand for 1 h before counting using a liquid scintillation counter (LKB Wallac 1215 Rackbeta). Each experimental curve is the average of three to eight independent experiments.

DNA Manipulations. The *T. versutus* AL2 *ccoNOQP* operon was amplified in parts and sequenced using a set of degenerate forward and reverse primers designed on the basis of multiple sequence alignments of the same operon of nine other proteobacterial species. DNA sequencing was performed in both directions using an automated, four-capillary DNA sequencer (ABI Prism 3100-Avant Genetic Analyzer) and an ABI Prism BigDye Terminator v. 3.1 reagent kit at the Genome Center of the Engelhardt Institute of Molecular Biology, Russian Academy of Sciences. Primary analyses of nucleotide sequences of the *ccoNOQP* genes were carried out using the BLASTA server. Sequences were aligned using the ClustalW program (5) and WebLogo software (6). The nucleotide sequence of the *ccoNOQP* of *T. versutus* AL2 has been deposited in the EMBL database (accession no. HE575403.1).

Heterologous Expression of *T. versutus* cbb_3 Oxidase in *P. denitrificans*. For cloning procedures, the *T. versutus* AL2 *ccoNOQP* operon was amplified by PCR using Pwo-polymerase (Roche Diagnostics) and the primer pair 5′-TTA AGC TTC AAG GTG GAA AAG TCA TGT CAC AAG-3′ (forward) and 5′-TTT CTA GAT TAC TGG CCG CCG CCC AAC GAA TG-3′ (reverse). Underlined bases in forward and reverse primers correspond to HindIII and XbaI restriction sites, respectively. The PCR fragment was cloned into the XbaI-HindIII–digested derivative of the broad host-range plasmid pBBR1MCS as described previously (2, 7) to produce the pBBR1/*ccoNOQP* plasmid. The nucleotide sequence of the cloned *ccoNOQP* was confirmed by sequencing the plasmid. For protein expression, the recombinant plasmid pBBR1/*ccoNOQP* was transferred by conjugation into the *Paracoccus* host strain AO1. The recipient, *P. denitrificans* AO1, expresses no cytochrome *c* oxidase activity (7). Exogenously expressed cbb_3 cytochrome *c* oxidase in strain AO1 usually reached a level comparable to that observed in the WT strain of *T. versutus* AL2, monitored using Western blotting. For Western blotting, membrane proteins were extracted from cytoplasmic membranes solubilized by stirring for 15 min at 4 °C in 30 mM Mops-HCl (pH 7.5), 0.5 mM EDTA, 5 mM NaCl, 0.7 M KCl, and *n*-octyl-β-D-glucopyranoside (0.5–1 g/g of total protein). Nonsolubilized components were sedimented and membrane proteins were separated by electrophoresis on 6% polyacrylamide gels under nondenaturating conditions (8) in the presence of 0.3% Triton X-100. Electrophoretically separated proteins were then electroblotted onto Hybond-P PVDF membranes (Amersham Pharmacia Biotech) at 14 V for 25 min in standard Towbin buffer (9) containing 0.1% SDS in a semidry transfer cell, as described by the manufacturer (Bio-Rad). Thereafter, blots were probed with polyclonal rabbit antibodies, and immunoreactive proteins were detected using an ECL Western blotting analysis system (Amersham Pharmacia BioTech). A BSA-conjugated, synthetic, 17-aa oligopeptide (KAEAREAQAASTEARTA) identical to the

C terminus of the *T. versutus* AL2 ccoN subunit was used for polyclonal rabbit antibody production.

Expression of Self-Coxs in WT *P. denitrificans*. In *P. denitrificans* WT strain grown aerobically (this study), expression of self-cbb_3 oxidase reached the same high level (100%) that was observed in this strain grown semiaerobically (3), as quantified by real-time quantitative PCR (qPCR); each self-Cox level, aa_3 and cbb_3, reached 70 pmol Cox/mg of membrane protein as determined by CO-reduced minus reduced spectra using extinction coefficients of 7 $mM^{-1}{\cdot}cm^{-1}$ (aa_3, 595–606 nm) (10) and 7.6 $mM^{-1}{\cdot}cm^{-1}$ (cbb_3, 558–572 nm) (as determined from spectra in ref. 11). The presence of both self-Coxs in WT *P. denitrificans* membranes, cbb_3 and aa_3, was confirmed independently by the laser flash-photolysis method (12, 13).

qPCR Experiments. Total RNA was isolated from 2 mL of bacterial suspension ($2.9{\cdot}10^9$ mL^{-1}) of WT *P. denitrificans* (strain PD 1222) using RNeasy Mini Kit (Qiagen) according to the manufacturer's protocol following by treatment with RNase-free DNase I (Fermentas). Total RNA was quantified at 260/280 nm using the NanoPhotometer P-Class (Implen) and stored at −70 °C. First-strand cDNA was synthesized using Revert Aid H minus first strand cDNA kit (Fermentas) with 1 μg of total RNA, following the manufacturer's instructions. A real-time PCR was performed using a DNA-Technology system with qPCR mix-HS SYBR (Evrogen). The two pairs of primers were used: 5′ccoN (TGTTGGACACCATCAAGCTGATCG) and 3′ccoN (AAGGCGATGACCACCCCGAC) for the N subunit of *P. denitrificans* cbb_3, and 5′Pden_1060 (ATGACCGGGCAGAAAATCAGGC) and 3′Pden_1060 (ACGATGTCGACACCCGACAGG) for *P. denitrificans* glyceraldehyde-3-phosphate dehydrogenase. To confirm that no genomic DNA was present in the RNA samples, cDNA was substituted with 1 μg of total RNA. Each sample was run in duplicate. The amplification was performed as follows: initial denaturation at 95 °C for 5 min, followed by 40 cycles of denaturation at 95 °C for 20 s, annealing at 59 °C for 20 s, and extension at 72 °C for 20 s. The relative expression levels of the *ccoN* gene were normalized to that of the Pden_1060 gene and calculated using the $2^{-\Delta\Delta Ct}$ method (14). The specificity of the PCR products was further verified by electrophoresis on a 1% agarose gel.

Amino Acid Sequence Determination. N-terminal amino acid sequences of polypeptides were determined as described previously (15).

Procedures for Recording Respiratory-Linked Activity. Respiratory activity of membranes was started by addition of substrate to the reaction mixture and was measured at 25 °C with an LP7e polarograph equipped with a standard platinum Clark-type electrode. The contribution of substrate autooxidation to the overall respiratory activity was assessed separately and subsequently subtracted from the obtained data.

HQNO pK_a Estimation. The pK_a values of HQNO-protonated groups were determined using ChemDBsoft (www.chemdbsoft.com).

Heme Analysis. Hemes were extracted (16) and separated by reversed-phase chromatography using a C18 column (Microbonda Sphere S-S; Waters).

Model Planar Membrane Experiments. Bilayer lipid membrane experiments were performed using a bilayer planar diphytanoyl phosphatidylcholine membrane, as described previously (17). The incubation mixture contained 10 mM KCl and 10 mM Tris buffer, pH 8.0. The experiment was started by adding KOH to one compartment to shift the pH in this compartment to 9.0.

Phylogenetic Analysis. A set of subunit I protein sequences representing the full phylogenetic divergence of the protein family was retrieved from GenBank. The sequences were aligned using Muscle 3.8 (18), and ambiguously aligned residues were removed with Gblocks (19). The resulting sequence block was used to estimate the phylogenetic tree with MrBayes 3.2 (20). Two parallel Bayesian analyses were started from random trees and run for 3 million generations. The consensus tree shown was built using data from the last 75% of the tree generations. The average SD of split frequencies between the two runs reached a value of 0.002, indicating excellent convergence of the runs. Our preliminary phylogenetic analyses using different combinations of sequences and parameter settings produced qualitatively similar results.

Model System and Molecular Dynamic Simulations. Simulation systems were prepared using SWISS-MODEL Workspace (21) and the software VMD (22). The structure of the cbb_3 H^+-motive oxidase (PDB ID code 3mk7), which has 69% sequence identity with the target, was used as a template for the model, allowing fully automated modeling. Two core subunits of the target, N and O, were built separately and then combined. The united model structure of the complex was embedded in a phospholipid bilayer, which included 1-palmitoyl-2-oleoyl-phosphatidylcholine (POPC) and cardiolipin (CLN) molecules, and solvated in a box of water molecules with a physiological concentration of NaCl (1 M). The final system consisted of the protein; 30, 12, and 5,207 molecules of POPC, CLN, and water, respectively; and 103 Na^+ and 70 chloride (Cl^-) ions to sustain electroneutrality. The charge distribution of the metal centers in cbb_3 Cox was parameterized according to a previously described protocol (23). In our model, assigned states "O" and "R" correspond to the described states III and II.

After the system was built, it was equilibrated in several stages. First, the coordinates of protein and lipid atoms were restrained and the system was equilibrated for 20 ns. Then, the lipid restraints were removed and equilibration was continued for 60 ns with 1 atm pressure coupling. Thereafter, the x, y and z dimensions of the simulation box were fixed at 61, 61, and 89 Å, respectively, and the protein was relaxed in a 120-ns MD simulation in which the restraints on the protein atoms were gradually reduced such that only a small (100 $kJ{\cdot}mol^{-1}{\cdot}nm^{-2}$) restraint was ultimately left on the C_α atoms of the protein backbone. This procedure was repeated separately for both Na^+- and H^+-motive forms of the enzyme. When redox or charged states of the protein were changed, an appropriate number of Na^+ or Cl^- ions was removed and the last stage of protein relaxation was repeated.

Protein in various redox and ionization states obtained by this procedure was used in subsequent free energy perturbation (FEP) and potential of mean force calculations. MD simulations were performed using the Gromacs package (version 4.5.5) (24) with the CHARMM36 force field (25). The temperature was kept at 303 K using the Nose–Hoover method. The Lennard-Jones interactions were switched off for distances greater than 1.2 nm with a switching distance of 1 nm. Periodic boundary conditions were performed using the particle-mesh Ewald method to calculate the electrostatic interactions without truncation. A time step of 2 fs was used in all MD simulations.

Free energy simulations: Evaluation of absolute ion binding affinities. FEP simulations were carried out with the standard Gromacs command using 21 windows (26) in accordance with the staged protocol of Deng and Roux (27). The binding free energies of Na^+ and Ca^{2+} ions were calculated using the equation $\Delta G_b = \Delta G_{\text{int}} + \Delta G_{tr}$, where the first term gives the free energy difference for the interactions of the ion with the environment

in the binding site and in the solution (i.e., the translocation energy), given by the algebraic expression

$$\Delta G = -\beta^{-1}\sum_{m=1}^{n-1}\ln\left\langle \exp\left[-\beta\frac{\partial V_m}{\partial\lambda_m}\Delta\lambda_m\right]\right\rangle_m ,$$

and the second term represents the free energy loss due to the reduction in translational entropy upon binding. The latter can be estimated from the root-mean-square fluctuations of the ion in the binding site $(\sigma_x, \sigma_y, \sigma_z)$ as $\Delta G_{tr} = -k_B T \ln[(2\pi e)^{3/2}\sigma_x\sigma_y\sigma_z/V_0]$, where $V_0 = 1.66$ nm^3, which is the reference volume for the standard concentration. The interaction energy was calculated using both the thermodynamic integration (TI) and FEP methods. The FEP method demonstrated a more effective convergence and thus was normally used. The simulation systems for the 21 windows were adapted from the preliminary TI calculation, where the transition $\lambda = (0\rightarrow1)$ occurred within 10 ns. Each window was then equilibrated for 0.5 ns, followed by a 0.5-ns or 1-ns production run. Convergence of free energy results was verified by doubling the production run time, which confirmed that sufficient sampling was obtained.

Initially, a Na^+ or Ca^{2+} ion was placed at the appropriate binding position in the protein and the system was equilibrated; a weak constraining potential was then applied to this ion. In addition, a neutral particle with the same van der Waals parameters was constrained in water far from the protein boundary. In forward calculations, the bound Na^+ (or Ca^{2+}) ion was alchemically transformed to a neutral atom while simultaneously transforming the neutral atom in bulk to a Na^+ (or Ca^{2+}) ion. After equilibrating in the forward direction, a backward transformation was performed, bringing the system back to the initial state with a bound ion. The binding free energy of an ion was determined from the average of forward and backward calculations.

U subunit building. Helix U in the united model structure was assigned to the ccoH sequence of *Pseudomonas stutzeri* cbb_3 (H7F0I7) using PyMOL software (28), taking into consideration descriptions provided in a previous study (29). The membrane-buried portion of the protein (N and U subunits) was solvated by water using the DOWSER program (30) as described previously (31). The molecular potentials for energy were taken from the standard CHARMM36 force field (25); an energy cutoff of −10 kcal/mol was used for water insertion. This procedure was repeated four times until protein saturation with water was reached.

SI Text

S1. Brief Characterization of the cbb_3 Cytochrome of *T. versutus* AL2. The cell membranes isolated from batch culture displayed highly active cytochrome *c*- and TMPD-supported respiration in the presence of a reductant ascorbate that was completely inhibited by cyanide (5 μM; Fig. S1*B*). The respiratory activity of membrane vesicles in the presence of reduced cytochrome *c* or reduced TMPD specifically depended on Na^+ concentration (Fig. 1 *A* and *B*). Apart from the *T. versutus* Cox, none of the H^+-motive Coxs, including *P. denitrificans* (WT strain) cbb_3 and aa_3 (Fig. S1 *A* and *B*), *Rhodobacter sphaeroides* cbb_3 (Fig. S1*C*), *P. stutzeri* cbb_3 (32), and bovine heart aa_3 (33), showed specific Na^+ activation. The difference absorption spectra of isolated cell membranes (reduction with sodium dithionite minus oxidation with air, or CO reduction with sodium dithionite minus reduction with sodium dithionite) (Fig. S4 *A* and *B*) together with HPLC heme analyses of cell membranes (Fig. S4*C*) showed that the cbb_3 cytochrome is the major terminal Cox of *T. versutus* AL2 under batch cultivation conditions.

The polyclonal rabbit antibodies produced against a polypeptide corresponding to the C terminus of the predicted cbb_3 oxidase catalytic subunit (*SI Materials and Methods*), ccoN (EMBL accession no. HE575403.1), reacted essentially with a single protein band in polyacrylamide gel after nondenaturating electrophoresis (PAGE; Fig. S5*A*). The second dimension SDS/PAGE electrophoresis of this protein band, eluted from the gel, revealed three subunits (the conventional subunit composition for cbb_3 oxidases) with apparent molecular weights of 48, 34, and 29 kDa (Fig. S5*B*, lane 3). Using antibodies against the C terminus of the predicted ccoN, we identified the 48-kDa polypeptide as the catalytic subunit (Fig. S5*B*, lanes 2 and 3), whereas the 29-kDa subunit was identified as ccoO based on the N-terminal amino acid sequence (Fig. S5*B*, lane 3 and inset). Staining gels by peroxidase heme reaction revealed that 34- and 29-kDa polypeptides contained covalently bound heme *c*. Thus, a cbb_3-type oxidase of a common subunit structure (34) was shown to be expressed in *T. versutus* AL2.

S2. HQNO Is an Alkaline Protonophore. Bacterial cells and vesicles were loaded with $^{22}Na^+$ to measure Na^+ efflux in response to respiration. Addition of substrate resulted in an efflux of Na^+ from *T. versutus* cells (Fig. 3*A*). The Δψ-dissipating compounds, CCCP and the K^+-ionophore valinomycin, activated this efflux from the cells. Similar results were obtained with closed right-side-out membrane vesicles from *T. versutus* as well as recombinant *P. denitrificans* after *T. versutus* cbb_3-type oxidase (Scox) expression, where Na^+ efflux was stimulated by valinomycin (Fig. 3 *B* and *D*). However, CCCP had little effect on Na^+ efflux from the vesicles. The pH both outside and inside of the vesicles was >9, which is considerably higher than pK_a of CCCP (6.0) and would lower the efficiency of this protonophore. Accordingly, we sought to replace CCCP with a protonophore with an alkaline pK_a. We found that HQNO [pK_a = 8.8 (*SI Materials and Methods*)], a weak protonophore at neutral pH (35) usually used as an inhibitor of the middle portion of the respiratory chain, acted as an effective protonophore in a model membrane at alkaline pH (Fig. S3*A*). Moreover, we showed that HQNO strongly stimulated respiratory activity in *T. versutus* AL2 cells, a property inherent in protonophores (Fig. S3*B*). In a subsequent experiment, we determined that HQNO strongly increased the rate of respiration-driven $^{22}Na^+$ extrusion from both cells and vesicles (Fig. 3 *A*, *B*, and *D*).

As to the Na^+-transport that followed operation of the *o*-type quinol oxidase from *Vitreoscilla* (36–41), the question on its primary or secondary character has not been clarified yet. The uncertainty rises because of the following reasons. (*i*) Activation of this Na^+ transport in synthetic proteoliposomes by uncouplers even at pH 7.6 was rather weak: When CCCP was used, 15–33% within four data points out of six and 60–100% within two points; when DTHB (3,5-di-*tert*-butyl-4-hydroxybenzaldehyde) was used, ±7% within four points and 50–65% within two points (36). (*ii*) At "zero" Na^+ concentration, curves of Na^+ dependence of activity start from about 50% of maximum activity meanings (37). (*iii*) Five millimolar cyanide only partly inhibited Na^+ transport activity and Δψ generation, namely by 30–50% (37, 38), although the *o*-type quinol oxidase was already inhibited by 50% in the presence of 8 μM cyanide (39). Consequently, data presented by Webster's group do not exclude the fact that during routine purification of the *o*-type oxidase authors obtained a mixture of at least two fractions of different enzymes. One of them could be sodium-activated whereas another one was indifferent with respect to Na^+ ions. Therefore, which of the two enzymes particularly was sodium-dependent is not clear. Apart from a routine method of protein purification, expression of the *o*-type oxidase in an appropriate host allows one to obtain membranes with this oxidase free of protein impurities deriving from *Vitreoscilla* cells, and in this case to find out by means of an uncoupler test whether the enzyme in question is a primary or secondary Na^+ pump. However, after this *o*-type oxidase was expressed in *Escherichia coli*, the effect of uncouplers was not tested (40, 41), which does not allow one to deduce unambiguously whether Na^+ was pumped primarily by that enzyme.

S3. Sodium-Conducting Pathway. cbb_3 Coxs are composed of the obligatory subunits N, O, and P, and an optional Q subunit. In H^+-motive cbb_3 Coxs, we predict a transient proton-conducting network at the interface between the catalytic subunit N and the additional auxiliary transmembrane α-helical polypeptide U ("subunit U") (Fig. 5*D*) (42). That subunit U definitely differs from subunit Q was revealed in the X-ray structure of *P. stutzeri* cbb_3 Cox, although its primary structure remained obscure. Here, we assigned the sequence of the additional subunit ccoH (*ccoH* expression product) (*SI Materials and Methods*) of the *P. stutzeri* cbb_3 Cox to helix U. This assignment is based on the following recent findings. (*i*) ccoH is a component of cbb_3 Coxs that were studied specially to find ccoH polypeptide; these cbb_3 Coxs include all detected isoforms of the *P. stutzeri* enzyme, recombinant cbb_3-1 and cbb_3-2, with high enzymatic activity (32), and the *Rhodobacter capsulatus* cbb_3 protein complex (29). (*ii*) ccoH is vital for cbb_3 Cox function. (*iii*) ccoH has the same secondary structure as helix U (29). Consequently, ccoH seems to be an obligatory small subunit of cbb_3 Coxs. Significantly, other minor polypeptides, ribosomal proteins and histone-like DNA-binding protein, that were detected in the *P. stutzeri* cbb_3 isoforms (32) have no transmembrane spanning helices and hence could not be considered as subunit U candidates. From the above, ccoH may be regarded as a possible candidate for the role of subunit U. In the *P. stutzeri* cbb_3 subunit N and U complex (NU), as so reconstituted, we detected a large solvent-accessible cavity located at the interface between helices IX–XI and U using PyMol software (Fig. 5*C*). This cavity continuously spans across the intramembrane part of the interhelix region from the cytoplasm boundary to the ionizable residue E323, a point two-thirds the depth of the membrane in the protein moiety. Using PyMol software, we found no other continuous cavity that could connect the cytoplasm and the ionizable residue E323 in the membrane domain of the *P. stutzeri* cbb_3 subunit N. Moreover, α-helices in subunit ccoN are so tightly packed that it is highly unlikely that they could contribute to translocation of ions other than H^+. Because the ccoN structure of *T. versutus* and *P. stutzeri* cbb_3 Coxs are highly homologous, we postulate that the *T. versutus* ccoN by itself has no sufficiently wide channel suitable for Na^+ translocation through the protein bulk. Although it is possible that the arrangement of N and U could allow Na^+ translocation through the cavity found at the interface of the two subunits, the hydrophobic properties of the inner surface of the cavity would not allow it to transfer ions without the presence of water in the cavity. To further investigate this possibility, we used the water prediction software DOWSER (30) to load water in the subunit NU complex of the *P. stutzeri* cbb_3 (*SI Materials and Methods*). In the water-loaded intersubunit NU cavity so obtained, the water network connects the cytoplasm in the vicinity of R308 with the buried residue E323 via a long water file (Fig. 5*D*). As shown in this model by the example of H^+ ions, the continuous water file could be a remarkable dynamic ion conductor (Fig. 5*D*, orange dashed line). As soon as the 3D structures of the both cbb_3 Coxs, H^+-motive from *P. stutzeri* and Na^+-motive from *T. versutus*, are highly identical, we assume that this ion translocation pathway is used in the Na^+-motive-like cbb_3 Coxs for Na^+ transfer. In the Na^+-motive-like cbb_3 Coxs, there is the L(M) substitution at position 308 compared with R(K)308 in the H^+-motive cbb_3 Coxs (Fig. S7), which could serve as a trap for Na^+ after dynamic narrowing of the channel entrance, thus ensuring ion selectivity at the cytoplasmic gate.

1. Sorokin DY, et al. (2001) *Thioalkalimicrobium aerophilum* gen. nov., sp. nov. and *Thioalkalimicrobium sibericum* sp. nov., and *Thioalkalivibrio versutus* gen. nov., sp. nov., *Thioalkalivibrio nitratis* sp.nov., novel and *Thioalkalivibrio denitrificancs* sp. nov., novel obligately alkaliphilic and obligately chemolithoautotrophic sulfur-oxidizing bacteria from soda lakes. *Int J Syst Evol Microbiol* 51(Pt 2):565–580.
2. Riistama S, Laakkonen L, Wikström M, Verkhovsky MI, Puustinen A (1999) The calcium binding site in cytochrome aa_3 from *Paracoccus denitrificans*. *Biochemistry* 38(33): 10670–10677.
3. Otten MF, Stork DM, Reijnders WN, Westerhoff HV, Van Spanning RJ (2001) Regulation of expression of terminal oxidases in *Paracoccus denitrificans*. *Eur J Biochem* 268(8):2486–2497.
4. Nakamura T, Tokuda H, Unemoto T (1982) Effects of pH and monovalent cations on the potassium ion exit from the marine bacterium, *Vibrio alginolyticus,* and the manipulation of cellular cation contents. *Biochim Biophys Acta* 692(3):389–396.
5. Thompson JD, Higgins DG, Gibson TJ (1994) CLUSTAL W: Improving the sensitivity of progressive multiple sequence alignment through sequence weighting, position-specific gap penalties and weight matrix choice. *Nucleic Acids Res* 22(22):4673–4680.
6. Crooks GE, Hon G, Chandonia JM, Brenner SE (2004) WebLogo: A sequence logo generator. *Genome Res* 14(6):1188–1190.
7. Pfitzner U, et al. (1998) Cytochrome *c* oxidase (heme aa_3) from *Paracoccus denitrificans*: Analysis of mutations in putative proton channels of subunit I. *J Bioenerg Biomembr* 30(1):89–97.
8. Davis BJ (1964) Disk electrophoresis – II. Method and application to human serum proteins. *Ann N Y Acad Sci* 121(2):404–427.
9. Towbin H, Staehelin T, Gordon J (1979) Electrophoretic transfer of proteins from polyacrylamide gels to nitrocellulose sheets: Procedure and some applications. *Proc Natl Acad Sci USA* 76(9):4350–4354.
10. Ludwig B, Schatz G (1980) A two-subunit cytochrome *c* oxidase (cytochrome aa_3) from *Paracoccus dentrificans*. *Proc Natl Acad Sci USA* 77(1):196–200.
11. García-Horsman JA, Berry E, Shapleigh JP, Alben JO, Gennis RB (1994) A novel cytochrome *c* oxidase from *Rhodobacter sphaeroides* that lacks CuA. *Biochemistry* 33(10): 3113–3119.
12. Muntyan MS, Dinarieva TY, Baev MV, Netrusov AI (2002) Effect of growth conditions on the synthesis of terminal oxidases in *Methylobacillus flagellatus* KT. *Arch Biochem Biophys* 398(1):118–124.
13. Muntyan MS, Bloch DA, Ustiyan VS, Drachev LA (1993) Kinetics of CO binding to H^+-motive oxidases of the caa_3-type from *Bacillus* FTU and of the *o*-type from *Escherichia coli*. *FEBS Lett* 327(3):351–354.
14. Livak KJ, Schmittgen TD (2001) Analysis of relative gene expression data using real-time quantitative PCR and the $2^{-\Delta\Delta\ CT}$ method. *Methods* 25(4):402–408.
15. Grinkevich VA, Lysenko AM, Muntyan MS, Skripnikova EV, Afrikyan EK (1997) Identification of *Bacillus* sp. FTU strain and the study of the caa_3-type oxidase homology. *Biochemistry (Mosc)* 62(7):718–724.
16. Sone N, Fujiwara Y (1991) Effects of aeration during growth of *Bacillus stearothermophilus* on proton pumping activity and change of terminal oxidases. *J Biochem* 110(6):1016–1021.
17. Severin FF, et al. (2010) Penetrating cation/fatty acid anion pair as a mitochondria-targeted protonophore. *Proc Natl Acad Sci USA* 107(2):663–668.
18. Edgar RC (2004) MUSCLE: Multiple sequence alignment with high accuracy and high throughput. *Nucleic Acids Res* 32(5):1792–1797.
19. Castresana J (2000) Selection of conserved blocks from multiple alignments for their use in phylogenetic analysis. *Mol Biol Evol* 17(4):540–552.
20. Ronquist F, Huelsenbeck JP (2003) MrBayes 3: Bayesian phylogenetic inference under mixed models. *Bioinformatics* 19(12):1572–1574.
21. Arnold K, Bordoli L, Kopp J, Schwede T (2006) The SWISS-MODEL workspace: A web-based environment for protein structure homology modelling. *Bioinformatics* 22(2): 195–201.
22. Humphrey W, Dalke A, Schulten K (1996) VMD: Visual molecular dynamics. *J Mol Graph* 14(1):33–38, 27–28.
23. Johansson MP, Kaila VRI, Laakkonen L (2008) Charge parameterization of the metal centers in cytochrome *c* oxidase. *J Comput Chem* 29(5):753–767.
24. Hess B, Kutzner C, van der Spoel D, Lindahl EJ (2008) GROMACS 4: Algorithms for highly efficient, load-balanced, and scalable molecular simulation. *J Chem Theory Comput* 4(3):435–447.
25. Brooks BR (1983) CHARMM: A program for macromolecular energy, minimization, and dynamics calculations. *J Comput Chem* 4(2):187–217.
26. Mark AE, van Helden SP, Smith PE, Janssen LHM, van Gunsteren WF (1994) Convergence properties of free energy calculations: α-cyclodextrin complexes as a case study. *J Am Chem Soc* 116(14):6293–6302.
27. Deng Y, Roux B (2009) Computations of standard binding free energies with molecular dynamics simulations. *J Phys Chem B* 113(8):2234–2246.
28. DeLano WL (2002) PyMOL Molecular Viewer. Available at www.pymol.org.
29. Ekici S, Pawlik G, Lohmeyer E, Koch H-G, Daldal F (2012) Biogenesis of cbb_3-type cytochrome *c* oxidase in *Rhodobacter capsulatus*. *Biochim Biophys Acta* 1817(6): 898–910.
30. Zhang L, Hermans J (1996) Hydrophilicity of cavities in proteins. *Proteins* 24(4): 433–438.
31. Sharma V, Wikström M, Kaila VRI (2012) Dynamic water networks in cytochrome cbb_3 oxidase. *Biochim Biophys Acta* 1817(5):726–734.
32. Xie H, Buschmann S, Langer JD, Ludwig B, Michel H (2014) Biochemical and biophysical characterization of the two isoforms of cbb_3-type cytochrome *c* oxidase from *Pseudomonas stutzeri*. *J Bacteriol* 196(2):472–482.
33. Bolli R, Nałecz KA, Azzi A (1985) The interconversion between monomeric and dimeric bovine heart cytochrome c oxidase. *Biochimie* 67(1):119–128.
34. Myllykallio H, Liebl U (2000) Dual role for cytochrome cbb_3 oxidase in clinically relevant proteobacteria? *Trends Microbiol* 8(12):542–543.

35. Krab K, Wikström M (1980) Effect of 2-n-heptyl-4-hydroxyquinoline N-oxide on proton permeability of the mitochondrial membrane. *Biochem J* 186(2):637–639.
36. Chung YT, Stark BC, Webster DA (2006) Role of Asp544 in subunit I for Na^+ pumping by *Vitreoscilla* cytochrome *bo*. *Biochem Biophys Res Commun* 348(4):1209–1214.
37. Kim SK, Stark BC, Webster DA (2005) Evidence that Na^+-pumping occurs through the D-channel in *Vitreoscilla* cytochrome *bo*. *Biochem Biophys Res Commun* 332(2):332–338.
38. Park C, Moon JY, Cokic P, Webster DA (1996) Na^+-translocating cytochrome *bo* terminal oxidase from *Vitreoscilla*: some parameters of its Na^+ pumping and orientation in synthetic vesicles. *Biochemistry* 35(36):11895–11900.
39. Efiok BJ, Webster DA (1990) A cytochrome that can pump sodium ion. *Biochem Biophys Res Commun* 173(1):370–375.
40. Efiok BJ, Webster DA (1990) Respiratory-driven Na^+ electrical potential in the bacterium *Vitreoscilla*. *Biochemistry* 29(19):4734–4739.
41. Georgiou CD, Cokic P, Carter K, Webster DA, Gennis RB (1988) Relationships between membrane-bound cytochrome *o* from *Vitreoscilla* and that of *Escherichia coli*. *Biochim Biophys Acta* 933(1):179–183.
42. Buschmann S, et al. (2010) The structure of cbb_3 cytochrome oxidase provides insights into proton pumping. *Science* 329(5989):327–330.

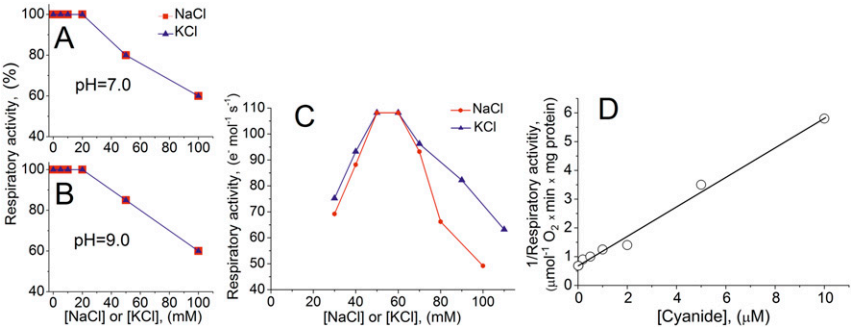

Fig. S1. Effects of monovalent cations (Na^+ and K^+) and cyanide on the respiratory activity of Coxs. (*A*–*C*) The dependence on monovalent cation concentration of respiratory activity (*A*) at pH = 7.0 and (*B*) pH = 9.0 of the H^+-motive self-cbb_3 and aa_3 Coxs presented in *P. denitrificans* (WT strain) membranes; each self-oxidase reached 70 pmol Cox·mg^{-1} of membrane protein; respiratory activity in the absence of exogenously added monovalent cations in each case, at pH = 7.0 (*A*) and pH = 9.0 (*B*), was defined as 100%; (*C*) of the isolated self-cbb_3 from *R. sphaeroides*. (*D*) Cyanide inhibition of respiratory activity in *T. versutus* membranes (semireciprocal coordinates). Incubation mixture: (*A* and *B*) 30 mM Mops-Tris (pH 7.0), 0.5 mM EDTA, or 30 mM CHES-Tris (pH 9.0), 0.5 mM EDTA (*C*) 30 mM Mops-Tris (pH 7.0), 0.5 mM EDTA, and 0.05% *n*-dodecyl β-D-maltoside; (*D*) 50 mM CHES-KOH (pH 9.5), 0.5 mM EDTA, and 100 mM NaCl. Respiratory substrates: 2 mM ascorbic acid and 6 μM horse heart cytochrome *c* (*A*–*C*); 2 mM ascorbic acid and 100 μM TMPD (*D*).

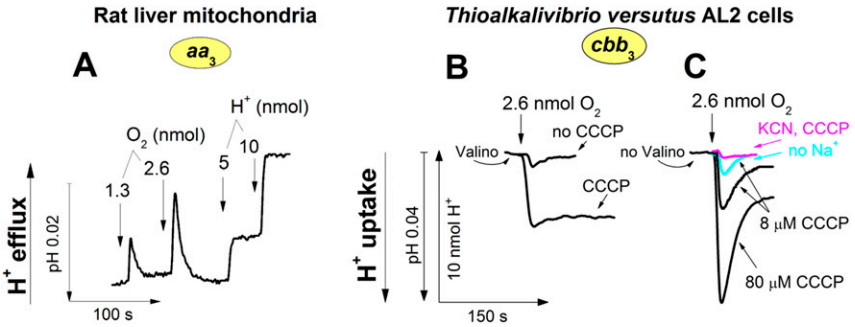

Fig. S2. The ion pumping activity of Coxs studied by various methods. (*A*) H^+ efflux and subsequent acidification of the external medium with rat liver mitochondria containing the aa_3-type Cox. (*B* and *C*) H^+ uptake and alkalinization of the external medium during operation of the cbb_3-type Cox in *T. versutus* AL2 cells. The reaction was initiated with O_2 pulse by injection of small aliquots of water into an anaerobic reaction mixture at pH 7.0 (*A*) or pH 9.0 (*B* and *C*). Basic incubation mixture (*A*–*C*): 0.12 M KCl, 10 mM ascorbate-KOH (pH 7), and 100 μM TMPD. In the case of *T. versutus* AL2 cells, incubation mixture was supplied with 0.5 M NaCl (*B* and *C*). Mitochondria or cells were incubated in the presence (*A* and *B*) or absence (*C*) of 1 μM valinomycin (valino) with or without 8 μM CCCP where indicated (*B* and *C*). Conditions in *C* additionally included 80 μM CCCP, CCCP (8 μM) + KCN (1 mM), CCCP (8 μM) + no Na (replaced with 0.5 M KCl), as indicated. Maximal H^+/e^- ratio for the O_2 pulse-induced H^+ uptake (alkalinization effect) in *T. versutus* AL2 cells was close to 0.8, supporting the assumption that the respiratory substrate was oxidized by a Na^+-motive oxidase that electrogenically transports one Na^+ ion per electron transferred from substrate to O_2. To evaluate alkalinization produced by Cox, we considered that ascorbate released 0.5 H^+/e^- in the reaction medium when donated electrons to Cox and this value should be subtracted from the overall pH change (1).

1. Wikström M, et al. (2005) Gating of proton and water transfer in the respiratory enzyme cytochrome c oxidase. *Proc Natl Acad Sci USA* 102(30):10478–10481.

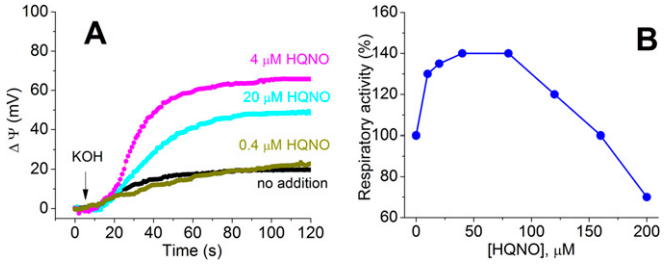

Fig. S3. HQNO properties as an alkaline protonophore. (*A*) An optimal HQNO concentration initiates a Nernstian H^+ diffusion potential across a bilayer lipid membrane (BLM). The incubation mixture contained 10 mM KCl and 10 mM Tris buffer, pH 8.0. The experiment was started by adding KOH to one compartment to shift the pH in this compartment to 9.0. Without HQNO, the pH gradient (ΔpH) formed did not generate a Δψ across the BLM, which is H^+-impermeable. However, addition of HQNO resulted in downhill, electrogenic transmembrane H^+ movement from the compartment of lower pH to that of higher pH, with the diffusion potential difference being about 60 mV per ΔpH unit (according to the Nernst equation). This Δψ was measured using two AgCl electrodes placed into the solutions on either side of the BLM (for method, see ref. 1). (*B*) HQNO stimulation of respiratory activity in *T. versutus* AL2 cells. Respiration was started by addition of the substrate NaHS (300 μM). The incubation mixture contained 50 mM CAPS-KOH (pH 10) and 0.6 M NaCl.

1. Severin FF, et al. (2010) Penetrating cation/fatty acid anion pair as a mitochondria-targeted protonophore. *Proc Natl Acad Sci USA* 107(2):663–668.

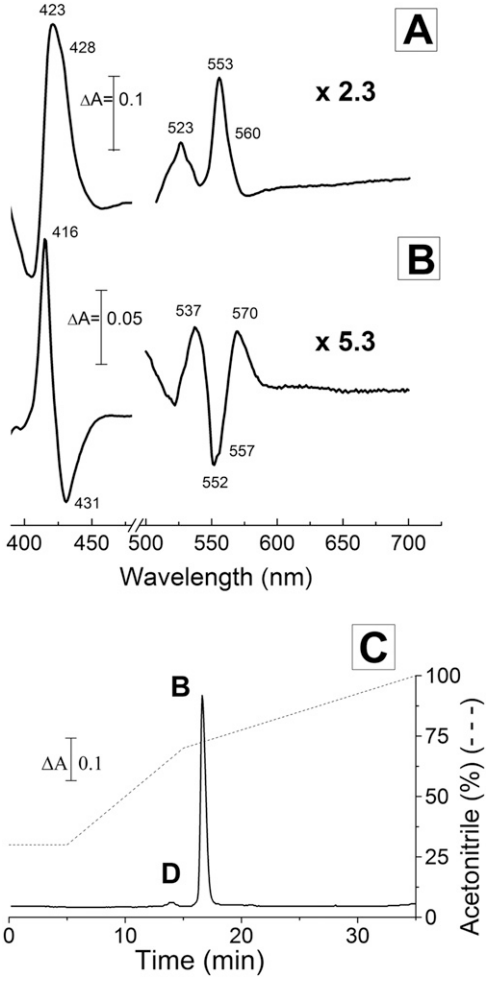

Fig. S4. Spectral and HPLC analysis of hemes in *T. versutus* membranes. (*A* and *B*) Visible absorption difference spectra: dithionite-reduced minus air-oxidized (*A*), and CO dithionite-reduced minus dithionite-reduced (*B*). (*C*) Heme composition of the membranes. The cells were grown at pH 10.0 as a batch culture. Hemes were extracted and separated by reversed-phase chromatography (*SI Materials and Methods*). The eluted compounds were detected by absorbance at 360 nm. D and B indicate the elution peaks of the corresponding hemes.

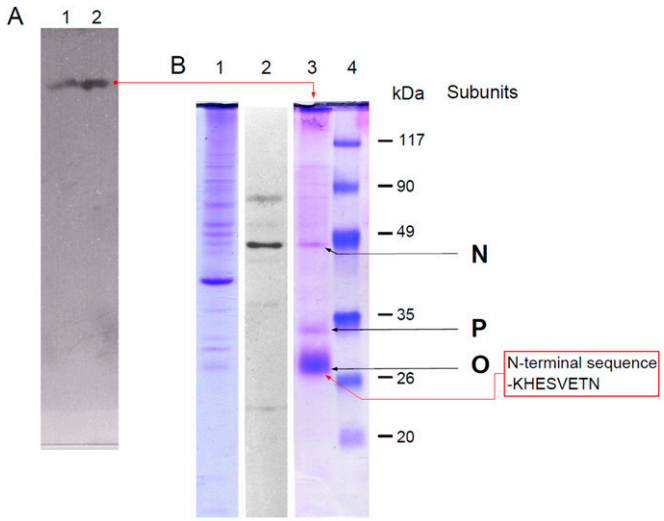

Fig. S5. Visualization of the *T. versutus* AL2 cbb_3 cytochrome *c* oxidase on polyacrylamide gels. (*A*) Representative Western blot of cbb_3 after native electrophoresis of the membrane protein extract in a 6% polyacrylamide gel, electroblotting, and probing with antibodies directed against the C terminus of the cbb_3 catalytic subunit (ccoN). Immunoreactive protein was detected by ECL. Lanes 1 and 2 correspond to 30- and 75-μg protein loads. (*B*) Electropherogram after SDS/PAGE on 12% gels. Lane 1, *T. versutus* AL2 membrane protein extract; lane 2, immunodetection of the *T. versutus* AL2 ccoN after denaturating gel electrophoresis of the membrane protein extract and electroblotting; lane 3, cbb_3 eluted from the band obtained from 6% nondenaturating gels detected by antibodies in immunoblots (*A*), as indicated by the upper red arrow; lane 4, molecular mass markers. Lanes 1, 3, and 4: Coomassie Brilliant Blue staining; lane 2, ECL detection of protein reactive to antibodies directed against the ccoN C terminus. The red-contoured inset shows the N-terminal sequence of the protein eluted from the band in lane 3 (lower red arrow). This sequence is identical to the N terminus of the translated O subunit (ccoO) of the *T. versutus* AL2 cbb_3 (EMBL accession no. HE575403.1). N, O, and P are the cbb_3 Cox obligatory subunits (1).

1. Myllykallio H, Liebl U (2000) Dual role for cytochrome cbb_3 oxidase in clinically relevant proteobacteria? *Trends Microbiol* 8(12):542–543.

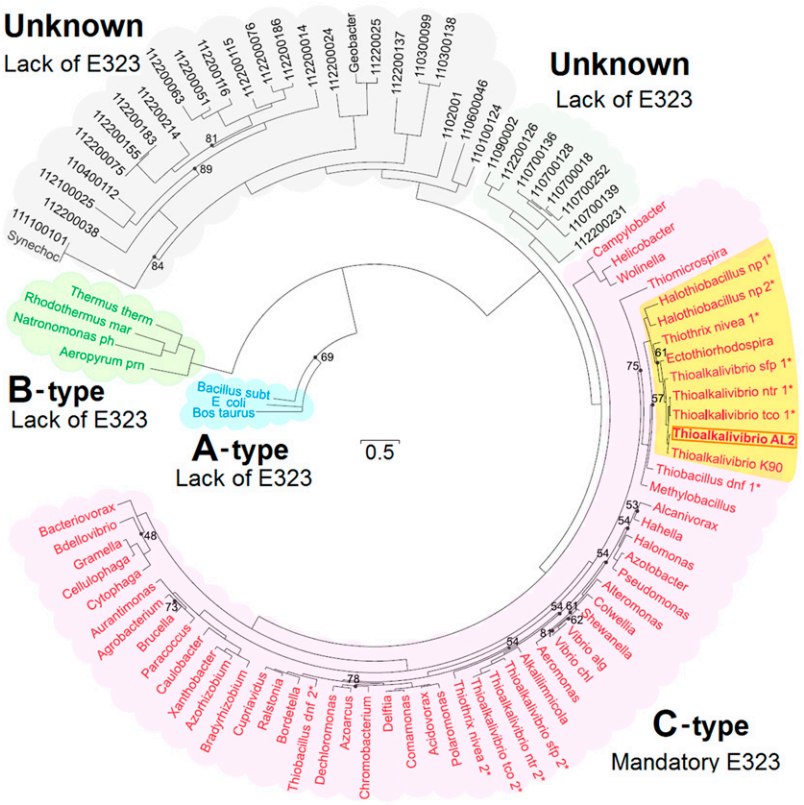

Fig. S6. Phylogenetic tree based on catalytic subunit protein sequences from representative Coxs (Table S1): A-type (blue), B-type (green), and C-type (red). *E. coli* o-type quinol oxidase is also shown (blue). E323 is specifically conserved in the catalytic subunit of C-type Coxs (see Fig. S7); residue numbering corresponds to *P. stutzeri* cbb_3 (here and elsewhere). The clade of Coxs with R(K)308L(M) substitution is yellow-colored; *T. versutus* cbb_3 Scox is orange-contoured. The sequences indicated in black (given in ref. 1) cluster separately from C-type Coxs (Unknown). Black spheres indicate nodes with clade credibility values <90; other nodes have clade credibility values ≥90. Asterisks indicate species with several operons for cbb_3 Cox in the genome. (Scale bar: 0.5 substitutions per residue.)

1. Hemp J, et al. (2007) Comparative genomics and site-directed mutagenesis support the existence of only one input channel for protons in the C-family (cbb_3 oxidase) of heme-copper oxygen reductases. *Biochemistry* 46(35):9963–9972.

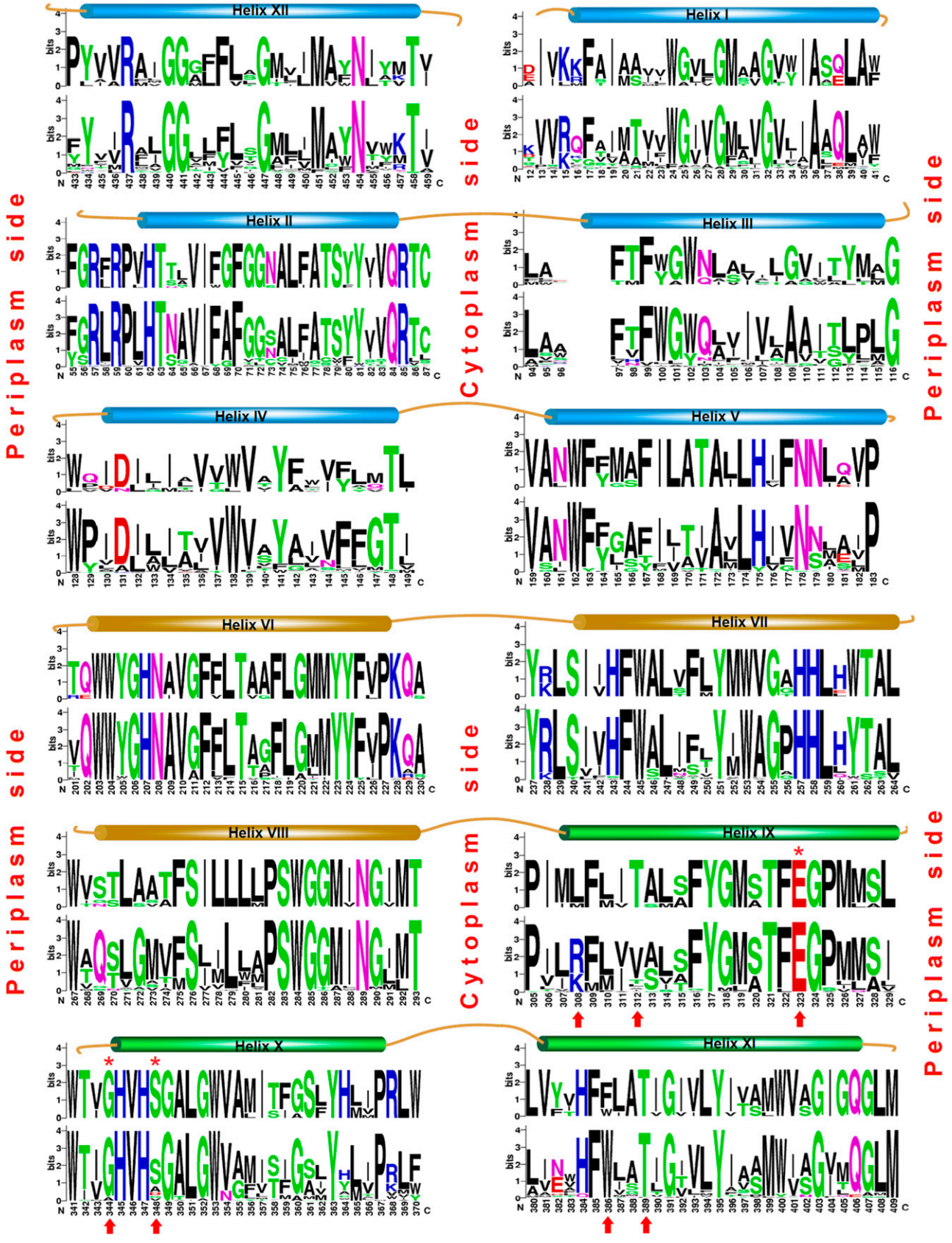

Fig. S7. Logo alignment of the amino acid sequences of the *cbb*$_3$ catalytic subunit of the two subgroups of C-type representatives: H^+- and Na^+-motive-like oxidases. The upper panels of each pair under an individual α-helix present a composite of representatives of the Na^+-motive-like *cbb*$_3$-oxidases (Fig. S6, yellow-highlighted clade in the C-type cluster), whereas the lower panels contain all other representatives of the C-type cluster (H^+-motive-like). A comparison of H^+- and Na^+-motive-like representatives showed no specific substitutions in the water-producing K-channel-analog region (VI–VIII helices, brown-colored). In

Legend continued on following page

contrast, the proposed ion-pumping channel region in the Na^+-motive-like representatives (IX–XI helices, green-colored) showed R(K)308 → L(M) substitution (red arrow). Red arrows show E323 conserved in both groups, W386 conserved only among H^+-motive-like representatives, and T312, G344, S348, and T389 conserved only among Na^+-motive-like representatives. Alignments were performed using WebLogo software (1). Red asterisks in the upper pannels (Na^+-motive-like template) indicate residues forming Na^+-coordination shell (shown in Fig. 5*B*).

1. Crooks GE, Hon G, Chandonia JM, Brenner SE (2004) WebLogo: A sequence logo generator. *Genome Res* 14(6):1188–1190.

Table S1. The bacterial cytochrome *c* oxidase sequences used to construct the phylogenetic tree in Fig. 4

Original name	Full name	GenBank protein sequence accession no.
Bacteriovorax	*Bacteriovorax marinus* SJ	YP_005035232
Bdellovibrio	*Bdellovibrio bacteriovorus* HD100	NP_969411
Gramella	*Gramella forsetii* KT0803	YP_861474
Cellulophaga	*Cellulophaga algicola* DSM 14237	YP_004164742
Cytophaga	*Cytophaga hutchinsonii* ATCC 33406	YP_677753
Aurantimonas	*Aurantimonas manganoxydans*	WP_009209598
Agrobacterium	*Agrobacterium fabrum* str. C58	NP_354541
Brucella	*Brucella melitensis* bv. 1 str. 16M	NP_540481
Paracoccus	*Paracoccus denitrificans* PD1222	YP_915641
Caulobacter	*Caulobacter* sp. K31	YP_001684062
Xanthobacter	*Xanthobacter autotrophicus* Py2	YP_001415374
Azorhizobium	*Azorhizobium caulinodans* ORS 571	YP_001527439
Bradyrhizobium	*Bradyrhizobium diazoefficiens* USDA 110	NP_769403
Thioalkalivibrio dnf 1	*Thiobacillus denitrificans* ATCC 25259	YP_314096
Methylobacillus	*Methylobacillus flagellatus* KT	YP_544740
Thioalkalivibrio tco 1	*Thioalkalivibrio thiocyanoxidans*	WP_006746787
Thioalkalivibrio ntr 1	*Thioalkalivibrio nitratireducens* DSM 14787	YP_007215385
Thioalkalivibrio K90mix	*Thioalkalivibrio* sp. K90mix	YP_003459410
Thioalkalivibrio AL2	*Thioalkalivibrio versutus* AL2	HE575403.1
Thioalkalivibrio sfp 1	*Thioalkalivibrio sulfidophilus* HL-EbGr7	YP_002515057
Ectothiorhodospira	*Ectothiorhodospira* sp. PHS-1	WP_008931898
Thiothrix nivea 1	*Thiothrix nivea*	WP_002710158
Halothiobacillus np 1	*Halothiobacillus neapolitanus* c2	YP_003263749
Halothiobacillus np 2	*Halothiobacillus neapolitanus* c2	YP_003263002
Cupriavidus	*Cupriavidus necator N*-1	YP_004686044
Ralstonia	*Ralstonia pickettii* 12J	YP_001898684
Bordetella	*Bordetella bronchiseptica* RB50	NP_889864
Thioalkalivibrio dnf 2	*Thiobacillus denitrificans* ATCC 25259	YP_314401
Dechloromonas	*Dechloromonas aromatica* RCB	YP_283939
Azoarcus	*Azoarcus* sp. BH72	YP_932845
Chromobacterium	*Chromobacterium violaceum* ATCC 12472	NP_900844
Delftia	*Delftia acidovorans* SPH-1	YP_001563798
Comamonas	*Comamonas testosteroni*	WP_003056324
Acidovorax	*Acidovorax citrulli* AAC00-1	YP_969886
Polaromonas	*Polaromonas* sp. JS666	YP_551095
Thiothrix nivea 2	*Thiothrix nivea*	WP_002710483
Thioalkalivibrio tco 2	*Thioalkalivibrio thiocyanoxidans*	WP_006748628
Thioalkalivibrio ntr 2	*Thioalkalivibrio nitratireducens* DSM 14787	YP_007217314
Thioalkalivibrio sfp 2	*Thioalkalivibrio sulfidophilus* HL-EbGr7	YP_002512712
Alkalilimnicola	*Alkalilimnicola ehrlichii* MLHE-1	YP_742716
Shewanella	*Shewanella baltica* OS155	YP_001041605
Vibrio chl	*Vibrio cholerae*	NP_231085
Vibrio alg	*Vibrio alginolyticus*	WP_005377474
Aeromonas	*Aeromonas hydrophila*	WP_011706146
Colwellia	*Colwellia psychrerythraea* 34H	YP_268725
Alteromonas	*Alteromonas macleodii* str. 'Deep ecotype'	YP_004427218
Pseudomonas	*Pseudomonas aeruginosa* PAO1	NP_252822
Azotobacter	*Azotobacter vinelandii* DJ	YP_002799183
Halomonas	*Halomonas maura*	AAY40171
Hahella	*Hahella chejuensis* KCTC 2396	YP_433526
Alcanivorax	*Alcanivorax borkumensis* SK2	YP_693071
Thiomicrospira	*Thiomicrospira crunogena* XCL-2	YP_392229
Wolinella	*Wolinella succinogenes* DSM 1740	NP_906440
Helicobacter	*Helicobacter acinonychis* str. Sheeba	YP_664165
Campylobacter	*Campylobacter coli*	WP_002779333
Geobacter	*Geobacter bemidjiensis* Bem	YP_002136948
Synechoc	*Synechococcus elongatus* PCC 6301	YP_172019
Thermus therm	*Thermus thermophilus* HB27	YP_004743
Rhodothermus mar	*Rhodothermus marinus* DSM 4252	YP_003290839
Natronomonas ph	*Natronomonas pharaonis*	CAA71525
Aeropyrum prn	*Aeropyrum pernix* K1	NP_148062
E. coli	*Escherichia coli*	WP_001601770
Bacillus subt	*Bacillus subtilis* subsp. *subtilis* str. 168	NP_389373
Bos taurus	*Bos taurus*	AAM08343

Table S2. Na^+-binding energy of the *cbb*$_3$-oxidase catalytic subunit estimated by the MD method

Protein		Charge states of *b*, b_3, Cu_B*	Na^+-binding center (E323)	
Function	Pump functional state		$\Delta G^{\dagger}$ (Na^+), kJ/mol	K_d, M
Sodium pump	Input‡	+2 +3 +1 (N 0 N)	−17	1.1×10^{-3}
	Output‡	+3 +3 +1 (0 0 N)	11.4	»6
Proton pump	Inactive	+2 +3 +1 (N 0 N)	6	»6
	Inactive	+3 +3 +1 (0 0 N)	27.6	»6

*In brackets are the relative charges (0 for uncharged, N for negatively charged) of the respective metallic centers (heme *b*, heme b_3, and Cu_B) with respect to the fully oxidized state of the enzyme (0 0 0). The (N 0 N) and (0 0 N) charge states of the enzyme are the main intermediates of the Na^+ pump; in the (N 0 N) state, an Na^+ ion crosses half the membrane interior from the cytoplasmic side and binds to E323 (input), whereas formation of the (0 0 N) state (which is coupled to binding of a "chemical" proton) causes Na^+ ejection to the periplasmic side of the membrane (output). The relevant input and output states were selected based on the following assumptions: (*i*) all transitions are one-electron; (*ii*) the reaction is thermodynamically favorable ($\Delta Ga < 0$) with a standard free energy change $\leq$ 25 kJ/mol; and (*iii*) $K_d(Na^+)$ is less than the typical Na^+ concentration in aqueous solutions. Residue numbering corresponds to the *P. stutzeri cbb*$_3$.

†SD of the mean was less than 2.8 kJ/mol.

‡The peripheral center at the periplasm–membrane interface contained Na^+.